LETTER

doi:10.1038/nature14364

Topological valley transport at bilayer graphene domain walls

Long Ju[1]*, Zhiwen Shi[1]*, Nityan Nair[1], Yinchuan Lv[1], Chenhao Jin[1], Jairo Velasco Jr[1], Claudia Ojeda-Aristizabal[1], Hans A. Bechtel[2], Michael C. Martin[2], Alex Zettl[1,3,4], James Analytis[1,3,4] & Feng Wang[1,3,4]

Electron valley, a degree of freedom that is analogous to spin, can lead to novel topological phases in bilayer graphene. A tunable bandgap can be induced in bilayer graphene by an external electric field[1–5], and such gapped bilayer graphene is predicted to be a topological insulating phase protected by no-valley mixing symmetry, featuring quantum valley Hall effects and chiral edge states[6–9]. Observation of such chiral edge states, however, is challenging because inter-valley scattering is induced by atomic-scale defects at real bilayer graphene edges[10]. Recent theoretical work[11–13] has shown that domain walls between AB- and BA-stacked bilayer graphene can support protected chiral edge states of quantum valley Hall insulators. Here we report an experimental observation of ballistic (that is, with no scattering of electrons) conducting channels at bilayer graphene domain walls. We employ near-field infrared nanometre-scale microscopy (nanoscopy)[14–16] to image *in situ* bilayer graphene layer-stacking domain walls on device substrates, and we fabricate dual-gated field effect transistors based on the domain walls. Unlike single-domain bilayer graphene, which shows gapped insulating behaviour under a vertical electrical field, bilayer graphene domain walls feature one-dimensional valley-polarized conducting channels with a ballistic length of about 400 nanometres at 4 kelvin. Such topologically protected one-dimensional chiral states at bilayer graphene domain walls open up opportunities for exploring unique topological phases and valley physics in graphene.

Hexagonal two-dimensional crystals, such as graphene and transition-metal dichalcogenides, exhibit a pair of degenerate bands at the K and K′ valleys in momentum space. The valley electrons are characterized by non-trivial Berry curvatures, which give rise to anomalous quantum Hall states in graphene[17] as well as valley Hall effects (the valley counterpart of spin Hall effects[18,19]). Bilayer graphene provides an attractive platform from which to explore topological valley physics[20]: a tunable semiconductor bandgap can be induced in bilayer graphene using a vertical electrical field, and different topological phases can exist in gapped bilayer graphene[6,7,11,21–23]. In particular, quantum valley Hall insulator states can exist in bilayer graphene (with any edge termination other than the armchair type) with a field-induced bandgap, where counterpropagating chiral electrons with opposite valley index exist at their boundaries[6–9]. Such one-dimensional chiral states are topologically protected as long as there are no inter-valley scatterings generated by atomic-scale defects.

Domain walls between AB- and BA-stacked bilayer graphene provide an attractive place to realize one-dimensional chiral boundary states of quantum valley Hall insulators because a smooth domain wall preserves the electron valley index in bilayer graphene, unlike valley-mixing atomic defects at graphene edges. The integrated Berry curvature of bilayer graphene valence bands for each valley is characterized by a quantized "valley" Chern number[11–13], the sign of which depends both on the direction of the vertical electrical field and the layer stacking order. Martin *et al.*[11] first proposed topological domain walls between band-inverted bilayer graphene insulators generated by opposite vertical electrical fields. Experimental realization of such electric-field walls, however, is extremely challenging. An alternative approach is to exploit different stacking orders. AB- and BA-stacked bilayer graphene under the same vertical electrical field represent two distinct topological phases with opposite valley Chern numbers. The stacking boundary between AB and BA domains forms a layer stacking domain wall (Fig. 1a). Valley-polarized chiral electrons are predicted[12,13] to flow along such a domain wall in gapped bilayer graphene, where K and K′ valley electrons propagate in opposite directions. Recent transmission electron microscopy studies show that smooth AB-BA domain walls with a width of several nanometres exist naturally in suspended bilayer graphene[24,25], but such suspended transmission electron microscopy bilayer graphene samples on through-holes (that is, holes that penetrate through a substrate) cannot easily be combined with bandgap control and transport measurements. Here we use a new approach to image *in situ* AB-BA domain walls in exfoliated (that is, prepared from graphite using tape) bilayer graphene on SiO_2/Si substrates, and demonstrate topologically protected charge and valley transport along such boundaries for the first time.

Few-layer graphene was mechanically exfoliated on 280-nm-thick SiO_2/Si substrates, and the layer thickness is determined using optical contrast measurements. To identify AB-BA layer stacking domain walls in bilayer graphene we used near-field infrared nanoscopy[14], as illustrated in Fig. 1b. Infrared light at 6.1 μm was focused onto the apex of a metal-coated atomic force microscope (AFM) tip with curvature radius $r \approx 25$ nm, and the scattered infrared radiation was collected and measured by an HgCdTe detector in the far field. The tip-enhanced infrared scattering provides a local probe of the material infrared responses with ~40 nm spatial resolution. The AB- and BA-stacked bilayer graphene, being inversion symmetric to each other, have exactly the same electronic bands and infrared absorption. The local band structure of the domain wall, however, is strongly modified relative to the bulk and exhibits different infrared contrast. Figure 1c and d displays AFM topography and near-field infrared nanoscopy images of the same bilayer graphene on a SiO_2/Si substrate. The bilayer graphene topography shows a step height of ~1 nm, consistent with the bilayer thickness. Within the bilayer graphene flake, the topography is featureless with a height fluctuation of less than 0.2 nm. In the near-field infrared nanoscopy image, however, distinct features appear in the bilayer graphene: multiple bright lines extend across the bilayer graphene flake and terminate at the edges. These bright lines in the infrared image indicate a change of local infrared conductivity in the bilayer graphene. No corresponding features can be discerned in the topography image (Fig. 1c), which excludes the possibility of surface contaminations or graphene folding along these lines. We attribute these local infrared response changes to AB-BA domain walls in bilayer graphene.

[1]Department of Physics, University of California, Berkeley, California 94720, USA. [2]Advanced Light Source Division, Lawrence Berkeley National Laboratory, Berkeley, California 94720, USA. [3]Materials Sciences Division, Lawrence Berkeley National Laboratory, Berkeley, California 94720, USA. [4]Kavli Energy NanoSciences Institute at the University of California, Berkeley and the Lawrence Berkeley National Laboratory, Berkeley, California 94720, USA.
*These authors contributed equally to this work.

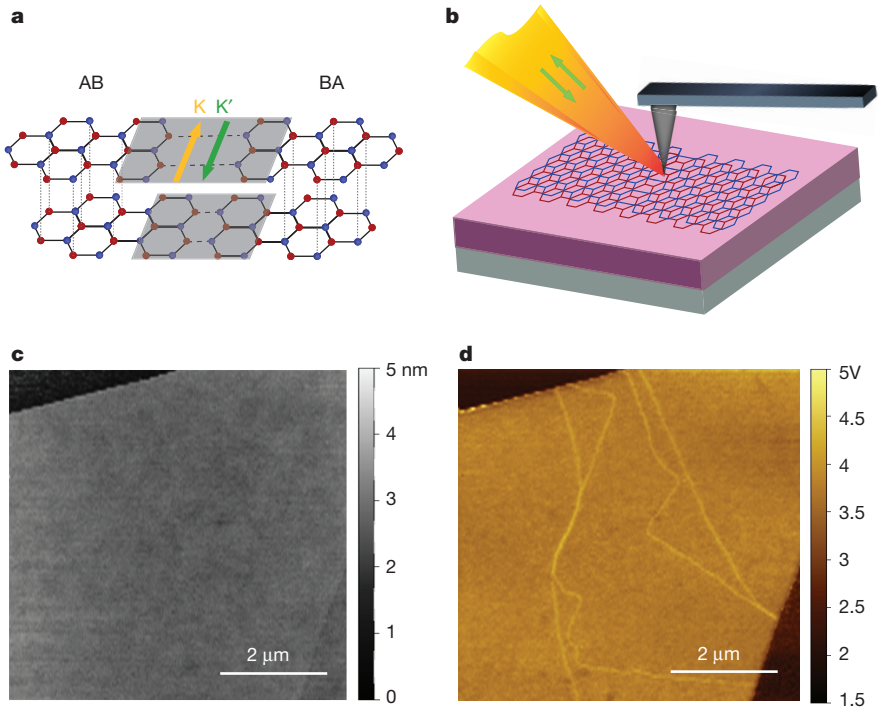

Figure 1 | Imaging AB-BA domain walls in exfoliated bilayer graphene. **a**, Illustration of a domain wall (shaded area) between AB- and BA-stacked bilayer graphene domains. The yellow (green) arrow indicates the one-dimensional conducting channel at the domain wall from K-valley (K′-valley) electrons. **b**, Illustration of the near-field infrared nanoscopy measurement of graphene on a SiO_2/Si substrate (pink/grey). Infrared light (yellow) at 6.1 μm was focused onto the apex of a metal-coated AFM tip and the backscattered infrared radiation was collected and measured by an HgCdTe detector in the far field. **c**, AFM topography map of a bilayer graphene sample on a SiO_2/Si substrate, showing no surface wrinkles or defects. (The small triangular area at the bottom right corner corresponds to a graphene monolayer.) **d**, Near-field infrared nanoscopy image of the same bilayer graphene sample as in **c**. Bright line features across the bilayer graphene flakes are observed that are absent in the topography image. These bright lines arise from AB-BA domain walls in bilayer graphene because the domain walls have different local electronic structure and infrared responses.

Qualitatively, we can approximate bilayer graphene in the domain wall region as randomly stacked bilayers, which has stronger local infrared response than bulk AB-stacked bilayer graphene and leads to the bright lines observed in infrared nanoscopy images (see Methods for details).

To confirm that the bright lines within the bilayer graphene are layer stacking domain walls, we systematically examined near-field infrared images of exfoliated graphene flakes of different layer thicknesses. Figure 2a–c shows infrared nanoscopy images of representative monolayer, bilayer, and trilayer graphene flakes, respectively. The infrared images of monolayers, like that in Fig. 2a, always show homogenous responses within the flake, although bright features can be observed parallel to the edges owing to the excitation of graphene plasmons. The absence of any structural domain boundary in monolayers is consistent with the high quality of the exfoliated samples. In bilayer graphene, about 30% of the exfoliated flakes show bright lines across the interior region of graphene like those in Fig. 2b, and areas between these lines have the same contrast. We identify these bright lines as AB-BA domain walls because they are the only one-dimensional structure that exists in bilayer but not monolayer graphene. This identification is further bolstered by the infrared images of graphene trilayers, such as that shown in Fig. 2c.

Bright lines extending through the graphene flakes are also observed, but unlike graphene bilayers, the domains separated by the bright lines can have different infrared contrast. This is because more domain stacking orders can exist in the trilayer, such as ABA, BAB, or ABC stacking. Although ABA and BAB domains are inversion symmetric to each other and have the same electronic structure, ABC domains have distinct band structures[26], infrared responses, and Raman spectra[27]. Therefore, a domain wall between ABA- and ABC-stacked trilayers will separate two domains having different infrared contrast in the near-field infrared image, as seen in domains I and II in Fig. 2c. In addition, we performed micro-Raman measurements on domains I and II, and show the corresponding spectra in Fig. 2d. It is apparent that the two-dimensional Raman features in domains I and II are different, and they have been shown to correspond to ABC- and ABA-stacked trilayer graphene[27], respectively. It demonstrates unambiguously that the bright line features in trilayers are layer stacking domain walls, and supports our assignment for bilayers.

After identifying the layer stacking domain walls in bilayer graphene on a SiO_2/Si substrate, we fabricated dual-gated bilayer field-effect transistor devices[4,5] across the domain walls. As references, we also fabricated dual-gated devices without domain walls using the same device configuration on the same bilayer graphene flakes. Figure 3a displays the optical microscopy image of a representative device. The white dashed line outlines the bilayer graphene flake, and the green line denotes the position of the AB-BA domain wall in the bilayer graphene. Source and drain electrodes (electrodes 1–5) composed of 40 nm Au and 0.5 nm Cr layers were defined by electron-beam lithography. Electrodes 1 and 2 are connected by a layer stacking domain wall, as are electrodes 2 and 3. Electrodes 3 and 4 and electrodes 4 and 5, on the other hand, are within a single bilayer graphene domain and act as reference devices. On top of the bilayer graphene flake, a 35-nm-thick Al_2O_3 dielectric layer was grown using atomic layer deposition. Last, the top gate electrodes of width 1 μm (TG1 and TG2) were patterned using electron-beam lithography and metal deposition. Figure 3b illustrates the side view of the device between electrodes 2 and 4, with a domain wall (green line) between electrodes 2 and 3 and single-domain bilayer graphene between electrodes 3 and 4. Here the doped silicon substrate acts as a bottom gate. By varying the top gate voltage V_{tg} and the bottom gate voltage V_{bg}, we can independently control the electric field above and below the bilayer graphene to generate a tunable semiconductor bandgap[5].

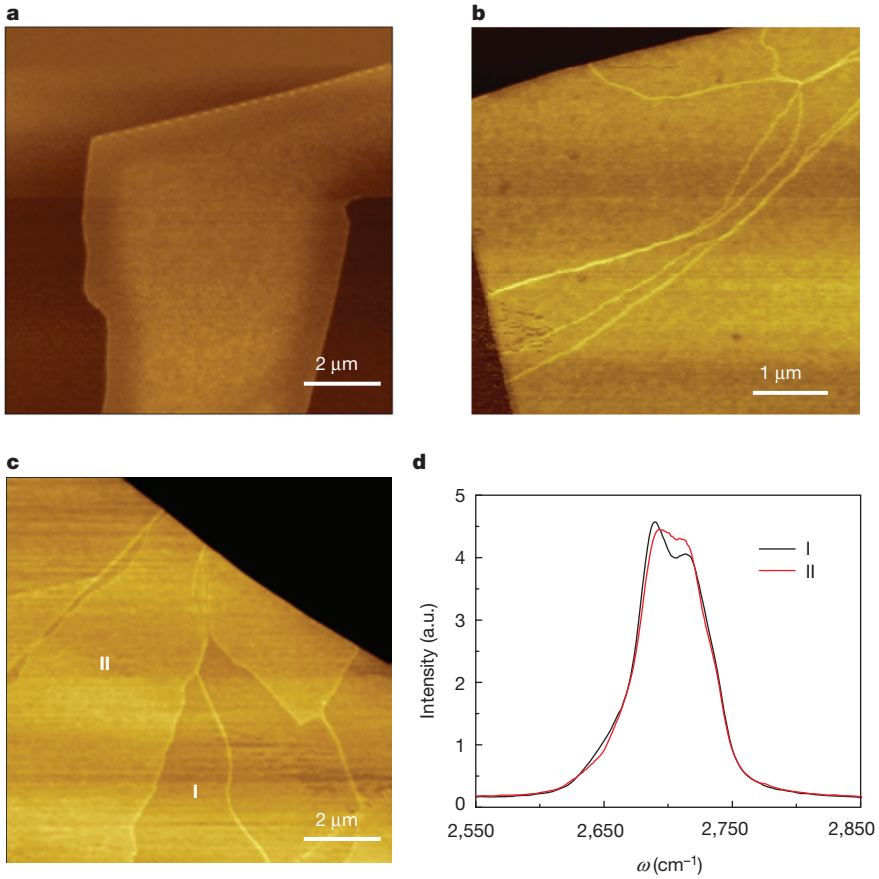

Figure 2 | Infrared nanoscopy images of domains and domain walls in exfoliated mono-, bi- and trilayer graphene. **a**, Infrared image of a graphene monolayer. The darker region corresponds to the SiO_2/Si substrate. Monolayer graphene shows homogeneous contrast across the whole sample with no bright lines in the interior area. (The bright lines parallel to the edge arise from plasmon excitations.) The same behaviour is observed in all exfoliated monolayers. **b**, Infrared image of a graphene bilayer, which shows bright line features across the flake. Such bright lines arise from AB-BA domain walls in bilayer graphene and they are observed in ~30% of exfoliated bilayer graphene samples. The bulk AB and BA domains have the same electronic structure and infrared contrast. **c**, Infrared image of a graphene trilayer, which exhibits domains with different infrared contrast as well as bright lines between domains. Different stacking orders, such as ABA and ABC stacking, can lead to different electronic structures and infrared contrast in trilayers. **d**, Raman spectra taken at domains I and II in **c**; ω is the Raman shift. The two-dimensional peak of domain I (black curve) and domain II (red curve) are characteristic of ABC and ABA stacking, respectively. It confirms that the bright and dark trilayer regions in **c** correspond to different layer stacking orders, and that the bright line features arise from layer stacking domain walls.

Figure 3c displays the electrical transport at 4 K in a reference bilayer graphene device without a domain wall. Each trace shows the gate-dependent resistance as a function of V_{tg} at a fixed bottom gate voltage, V_{bg}. V_{bg} was varied in steps of 10 V to produce the different traces. The resistance peak in each trace corresponds to a charge neutral point (CNP), at which the Fermi level resides within the semiconductor bandgap. CNPs can be realized with different combinations of V_{tg} and V_{bg}, but each with a different vertical electrical field and induced semiconductor bandgap in bilayer graphene. The zero-bandgap state is realized at $V_{bg}^{0} = 0$ V and $V_{tg}^{0} = 1.8$ V, which has the lowest peak resistance. The average displacement field[5] across bilayer graphene is described by $D = \frac{1}{2}(D_b + D_t)$. Here $D_b = \varepsilon_{SiO_2}\left|V_{bg} - V_{bg}^{0}\right|/d_{SiO_2}$, and $D_t = \varepsilon_{Al_2O_3}\left|V_{tg} - V_{tg}^{0}\right|/d_{Al_2O_3}$, where ε and d are the dielectric constant and thickness of the respective oxide dielectric layers. The bandgap increases monotonically with the average vertical displacement field D, which results in a larger peak resistance at the CNP. The experimental values of the peak resistances are lower than that expected from the semiconductor bandgap in ideal bilayer graphene, presumably owing to impurities and defects in our devices. Nevertheless, the resistance can reach ~90 kΩ at 4.2 K, similar to that observed in previous dual-gated bilayer graphene devices on SiO_2/Si substrates[4].

Electrical transport through bilayer graphene with an AB-BA domain wall exhibits a different behaviour, as shown in Fig. 3d. When the bilayer graphene bandgap is small (purple traces), the gate-dependent resistance curves are similar to those in single-domain bilayer graphene devices because bulk current flowing through the domain dominates. With higher displacement fields and larger bilayer graphene bandgaps, the peak resistance in each curve first increases and then saturates at ~14 kΩ (red traces in Fig. 3d), in striking contrast to the monotonically increasing resistance to over 80 kΩ in the reference device without a domain wall (Fig. 3c). Figure 4a plots the comparison of bilayer graphene peak resistances in the device with a domain wall (red circles) and without a domain wall (black squares) as a function of the vertical displacement field D, explicitly showing that saturation of the peak resistances occurs at a much lower value, owing to the presence of the domain wall.

These distinct transport behaviours in bilayer graphene with and without AB-BA domain walls were observed in all of the bilayer graphene devices that we studied (see Methods for details.) It is apparent that the conductance is always much higher in bilayer graphene devices with AB-BA domain walls. In addition, we performed temperature dependence studies of CNP resistance in bilayer graphene with and without domain walls from 1.8 K to 50 K. We observed that the resistance of bulk bilayer graphene increases many times at lower temperature, characteristic of an insulating phase. The resistance across the domain wall, however, behaves like a metallic system with much weaker temperature dependence (see Methods for details). Our results demonstrate unambiguously that one-dimensional conducting

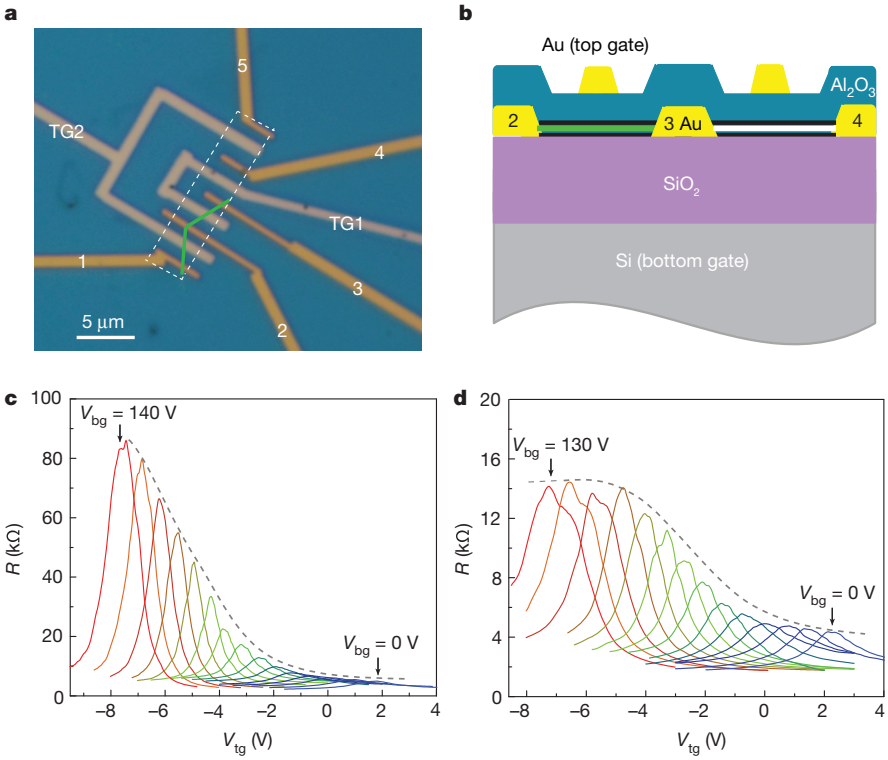

Figure 3 | Dual-gated field-effect transistor devices on bilayer graphene with AB-BA domain walls and their electrical transport properties. **a**, Optical micrograph of a dual-gated bilayer device. The white dotted line outlines the bilayer graphene flake, and the green line denotes the AB-BA domain wall. Source and drain electrodes are labelled from 1 to 5. Electrodes 1 and 2 are connected by a layer stacking domain wall, as are electrodes 2 and 3. Electrodes 3 and 4 and electrodes 4 and 5, on the other hand, are within a single bilayer graphene domain and act as reference devices. TG1 and TG2 denote top gate electrodes. **b**, Side view of the dual-gated bilayer device between electrodes 2 and 4 in **a**. **c**, Gate-dependent resistance for bilayer graphene without a domain boundary (electrodes 3 and 4). The backgate voltage V_{bg} is varied from 0 V to 140 V with a step of 10 V (colours here and in **d** indicate different curves), and the top gate voltage V_{tg} is swept continuously. The resistance peak in each trace corresponds to a CNP. The resistance at the CNP increases continuously (dashed grey line) to over 80 kΩ at high V_{bg} owing to the opening of a bandgap. **d**, Gate-dependent resistance across bilayer graphene with a domain boundary (electrodes 2 and 3). The resistance at the CNP first increases and then saturates at ~14 kΩ, although the bilayer graphene bandgap keeps increasing with increasing V_{bg}. This much lower resistance signifies the presence of a one-dimensional conducting channel at the AB-BA domain wall.

channels are present at the AB-BA domain walls, and that they dominate the electrical transport when bulk bilayer graphene domains become insulating.

To examine the conducting channels through the bilayer graphene domain walls, we systematically investigated bilayer graphene devices with varying channel length (defined by the top gate width) along the same bilayer graphene domain wall. Figure 4b displays the measured conductance of the two sets of bilayer graphene domain wall channels with lengths of 200 nm, 400 nm, 600 nm and 800 nm, respectively and another batch of 1,000-nm-long bilayer graphene domain wall channels. All the conductance values are of the order of the quantum conductance ($2e^2/h$, where e is the unit charge and h is Planck's constant), and one of the shortest channels exhibits a conductance approaching $4e^2/h$.

The observed one-dimensional conducting channels correspond to the chiral edge modes at AB-BA domain walls recently predicted by theory[11–13]. Figure 4c shows the electronic band structure around the K and K′ points for bilayer graphene with an AB-BA domain wall. In gapped bilayer graphene, the AB- and BA-stacked domains represent two different quantum valley Hall insulators. Consequently, a domain wall separating insulating AB and BA domains will confine a pair of one-dimensional conducting channels along the boundary for each valley. The conducting electrons in different valleys have opposite energy dispersions, and therefore propagate with opposite velocities. Such counter-propagating, valley-projected chiral electrons along the AB-BA domain walls are illustrated in Fig. 4d in real space. These conducting chiral modes are topologically protected within a single valley. Inter-valley scatterings can potentially mix the forward- and backward-moving electrons and eliminate the chiral modes, analogous to magnetic impurities that flip spins and eliminate chiral modes in quantum spin Hall insulators. However, at atomic-defect-free AB-BA domain walls where the crystal lattice is smoothly varying, such inter-valley scattering will be absent because it requires a large momentum change of $4\pi/\left(3\sqrt{3}\right)a_{c-c}$, where $a_{c\text{-}c}$ is the carbon–carbon bond length of 1.42 Å.

We can quantitatively compare the observed one-dimensional conductance along the AB-BA domain wall with theoretical predictions. As illustrated in Fig. 4d, two conducting chiral modes are present at the domain wall for a given current flow direction. In addition, each chiral mode is doubly degenerate owing to electron spin. Therefore, four one-dimensional conducting channels exist at the domain wall, giving an ideal conductance of $4e^2/h$, that is, two conductance quanta. Experimentally, we observed conductance of the order of the conductance quanta in all devices, and one 200-nm-long domain wall channel exhibits conductance close to the value of $4e^2/h$ (Fig. 4b). We found that overall the one-dimensional channel conductance becomes lower with increasing channel length. The observed length-dependent conductance through bilayer graphene domain walls can be described by the Landauer–Büttiker formula[28] with a finite electron mean free path: $G=\left(R_c+R_0\left(1+\frac{L}{L_0}\right)\right)^{-1}$, where L is the channel length, $R_0=h/4e^2$, the contact resistance $R_c=0$, and the mean free path $L_0=420$ nm (solid line in Fig. 4b). The electron mean free path of 420 nm can arise from a finite inter-valley scattering along the bilayer graphene domain walls, and previous transport studies have reported a comparable inter-valley scattering length of 300–800 nm in bilayer graphene on SiO_2/Si substrates[29]. Nevertheless, this electron mean free path along the bilayer graphene domain wall is orders of magnitude longer than

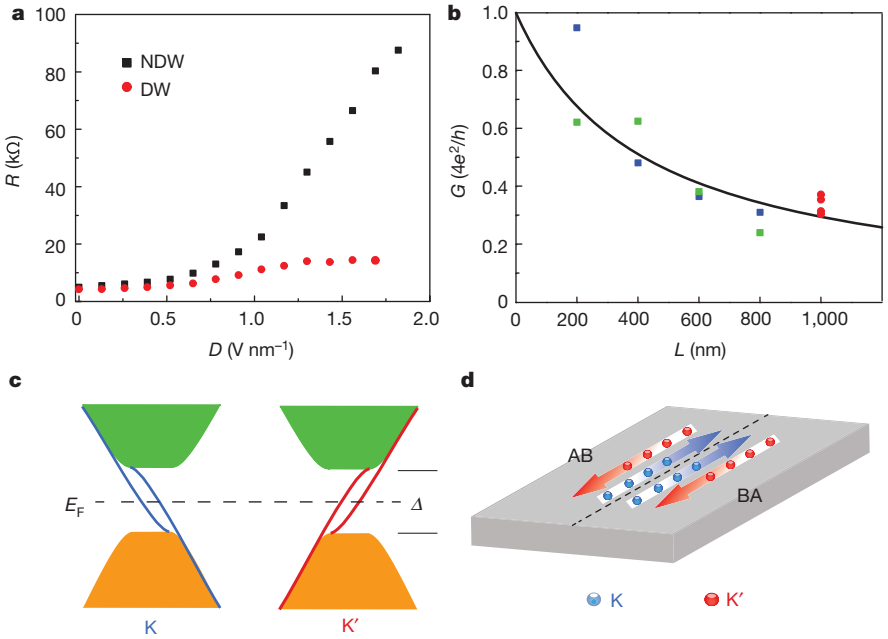

Figure 4 | Conductivity of topologically protected chiral modes at AB-BA domain walls. **a**, CNP resistances as a function of displacement field D for bilayer graphene with no domain wall (NDW, black squares) and for bilayer graphene with a domain wall (DW, red circles) obtained from Fig. 3. The saturation of the resistance at a much lower value at high D originates from one-dimensional conducting channels at the domain wall. **b**, Length dependence of the bilayer graphene domain wall conductance. Green and blue symbols represent two sets of devices, each fabricated on one single domain wall in the same bilayer graphene flake. Red symbols represent another batch of 1,000-nm-long domain wall channels. All devices exhibit conductance of the order of the quantum conductance, with lower conductance in longer channels and a maximum conductance approaching $4e^2/h$. This length-dependent one-dimensional conductance can be described by four conducting channels with a mean free path of 420 nm using the Landauer–Büttiker formula (solid line). **c**, Electronic band structure of bilayer graphene with an AB-BA domain wall. Solid green and orange regions represent states of the bulk bilayer with a bandgap of Δ, E_F indicates the Fermi energy, and the blue (red) lines represent topologically protected K-valley (K′-valley) chiral electron modes at the domain wall. Each chiral electron mode is doubly spin degenerate, leading to four valley-polarized one-dimensional conducting channels at the AB-BA domain wall of a gapped bilayer graphene sample. **d**, Illustration of valley-polarized electrical current at the bilayer graphene AB-BA domain wall. Boundary states in the K and K′ valley move in opposite one-way channels, leading to ballistic charge and valley current along the domain wall.

that in the bilayer graphene domain, which has a mobility of $\sim$2,000 cm^2 V^{-1} s^{-1} and a mean free path of only $\sim$8 nm in our samples. In general, scattering and localization effects tend to be more important in one dimension. The much longer mean free path at the AB-BA domain walls therefore highlights the topological protection of chiral electron modes, where the electron velocity-valley locking forbids intra-valley backscattering. Because inter-valley scattering along the smooth domain walls is negligible, the chiral valley channels at AB-BA domain walls are very robust even for bilayer graphene devices on SiO_2/Si substrates. We envision that encapsulation in boron nitride layers[30] could potentially lead to chiral electrons at AB-BA domain walls with very long coherent lengths.

Our observation of topologically protected one-dimensional conducting channels at bilayer graphene domain walls opens up exciting opportunities to explore tunable topological phases and valley physics in graphene. Owing to the velocity-valley locking, the one-dimensional chiral modes at the AB-BA domain walls lead not only to ballistic charge transport, but also to ballistic valley transport. Such chiral modes can enable novel ways to control the valley degree of freedom for valleytronic devices based on bilayer graphene.

Online Content Methods, along with any additional Extended Data display items and Source Data, are available in the online version of the paper; references unique to these sections appear only in the online paper.

Received 27 October 2014; accepted 25 February 2015.
Published online 22 April 2015.

1. McCann, E. Asymmetry gap in the electronic band structure of bilayer graphene. *Phys. Rev. B* **74,** 161403 (2006).
2. Castro, E. V. *et al.* Biased bilayer graphene: semiconductor with a gap tunable by the electric field effect. *Phys. Rev. Lett.* **99,** 216802 (2007).
3. Min, H. K., Sahu, B., Banerjee, S. K. & MacDonald, A. H. *Ab initio* theory of gate induced gaps in graphene bilayers. *Phys. Rev. B* **75,** 155115 (2007).
4. Oostinga, J. B., Heersche, H. B., Liu, X. L., Morpurgo, A. F. & Vandersypen, L. M. K. Gate-induced insulating state in bilayer graphene devices. *Nature Mater.* **7,** 151–157 (2008).
5. Zhang, Y. B. *et al.* Direct observation of a widely tunable bandgap in bilayer graphene. *Nature* **459,** 820–823 (2009).
6. Yao, W., Yang, S. A. & Niu, Q. Edge states in graphene: from gapped flat-band to gapless chiral modes. *Phys. Rev. Lett.* **102,** 096801 (2009).
7. Zhang, F., Jung, J., Fiete, G. A., Niu, Q. A. & MacDonald, A. H. Spontaneous quantum Hall states in chirally stacked few-layer graphene systems. *Phys. Rev. Lett.* **106,** 156801 (2011).
8. Castro Neto, A. H., Guinea, F., Peres, N. M. R., Novoselov, K. S. & Geim, A. K. The electronic properties of graphene. *Rev. Mod. Phys.* **81,** 109 (2009).
9. Jung, J., Zhang, F., Qiao, Z. H. & MacDonald, A. H. Valley-Hall kink and edge states in multilayer graphene. *Phys. Rev. B* **84,** 075418 (2011).
10. Yan, J. & Fuhrer, M. S. Charge transport in dual gated bilayer graphene with Corbino geometry. *Nano Lett.* **10,** 4521–4525 (2010).
11. Martin, I., Blanter, Y. M. & Morpurgo, A. F. Topological confinement in bilayer graphene. *Phys. Rev. Lett.* **100,** 036804 (2008).
12. Zhang, F., MacDonald, A. H. & Mele, E. J. Valley Chern numbers and boundary modes in gapped bilayer graphene. *Proc. Natl Acad. Sci. USA* **110,** 10546–10551 (2013).
13. Vaezi, A., Liang, Y. F., Ngai, D. H., Yang, L. & Kim, E. A. Topological edge states at a tilt boundary in gated multilayer graphene. *Phys. Rev. X* **3,** 021018 (2013).
14. Keilmann, F. & Hillenbrand, R. Near-field microscopy by elastic light scattering from a tip. *Phil. Trans. R. Soc. A* **362,** 787–805 (2004).
15. Chen, J. N. *et al.* Optical nano-imaging of gate-tunable graphene plasmons. *Nature* **487,** 77–81 (2012).
16. Fei, Z. *et al.* Gate-tuning of graphene plasmons revealed by infrared nano-imaging. *Nature* **487,** 82–85 (2012).
17. Novoselov, K. S. *et al.* Unconventional quantum Hall effect and Berry's phase of 2π in bilayer graphene. *Nature Phys.* **2,** 177–180 (2006).
18. Kane, C. L. & Mele, E. J. Quantum spin Hall effect in graphene. *Phys. Rev. Lett.* **95,** 226801 (2005).
19. Konig, M. *et al.* Quantum spin hall insulator state in HgTe quantum wells. *Science* **318,** 766–770 (2007).
20. Wen, X. G. Symmetry-protected topological phases in noninteracting fermion systems. *Phys. Rev. B* **85,** 085103 (2012).

21. Weitz, R. T., Allen, M. T., Feldman, B. E., Martin, J. & Yacoby, A. Broken-symmetry states in doubly gated suspended bilayer graphene. *Science* **330,** 812–816 (2010).
22. Velasco, J. *et al.* Transport spectroscopy of symmetry-broken insulating states in bilayer graphene. *Nature Nanotechnol.* **7,** 156–160 (2012).
23. Maher, P. *et al.* Evidence for a spin phase transition at charge neutrality in bilayer graphene. *Nature Phys.* **9,** 154–158 (2013).
24. Alden, J. S. *et al.* Strain solitons and topological defects in bilayer graphene. *Proc. Natl Acad. Sci. USA* **110,** 11256–11260 (2013).
25. Butz, B. *et al.* Dislocations in bilayer graphene. *Nature* **505,** 533–537 (2013).
26. Min, H. K. & MacDonald, A. H. Electronic structure of multilayer graphene. *Prog. Theor. Phys.* **176** (Suppl.), 227–252 (2008).
27. Lui, C. H. *et al.* Imaging stacking order in few-layer graphene. *Nano Lett.* **11,** 164–169 (2011).
28. Datta, S. *Electronic Transport in Mesoscopic Systems* Ch. 2 (Cambridge Univ. Press, 1995).
29. Gorbachev, R. V., Tikhonenko, F. V., Mayorov, A. S., Horsell, D. W. & Savchenko, A. K. Weak localization in bilayer graphene. *Phys. Rev. Lett.* **98,** 176805 (2007).
30. Wang, L. *et al.* One-dimensional electrical contact to a two-dimensional material. *Science* **342,** 614–617 (2013).

Acknowledgements We thank Y. Ye and H. Zhu for their help on electron-beam lithography, Y. Zeng and H. Chang for help with device fabrication, and M. Raschke for help with near-field infrared techniques. The optical and electrical measurements were supported by the Office of Basic Energy Science, Department of Energy under contract numbers DE-SC0003949 (Early Career Award), DE-AC02-05CH11231 (Materials Science Division SP2 programme and the Laboratory Directed Research and Development Program of Lawrence Berkeley National Laboratory). Device fabrication was supported by the Office of Naval Research (award N00014-13-1-0464). F.W. acknowledges support from a David and Lucile Packard fellowship. The Advanced Light Source is supported by the Director, Office of Science, Office of Basic Energy Sciences, of the US Department of Energy under contract number DE-AC02-05CH11231.

Author Contributions F.W., L.J. and Z.S conceived the experiment, Z.S., C.J., H.A.B. and M.C.M. performed the near-field infrared nanoscopy and optical measurements, L.J., Y.L. and J.V. fabricated the dual-gated field-effect transistor devices, L.J., N.N. and C.O.-A. did the electrical transport measurements. F.W., J.A. and A.Z. supervised the project. All authors discussed the results and wrote the paper.

Author Information Reprints and permissions information is available at www.nature.com/reprints. The authors declare no competing financial interests. Readers are welcome to comment on the online version of the paper. Correspondence and requests for materials should be addressed to F.W. (fengwang76@berkeley.edu).

METHODS

Mechanism of the infrared contrast for domain walls. Our near-field infrared nanoscopy probes the local optical conductivity at infrared frequencies with ~40 nm spatial resolution. The infrared contrast of the domain wall arises from its different electronic structure and infrared conductivity from the AB-stacked bilayer graphene. An exact description of the local band structure of a domain wall is beyond the scope of this work. However, the domain wall region is characterized by shifted top and bottom layers, which can be approximated by two randomly stacked monolayers of graphene. Such randomly stacked graphene has electronic structure similar to that of two separated monolayers close to the Dirac point[31], and its infrared conductivity can be approximated by $2\sigma_{monolayer}$. The AB-stacked bilayer graphene, on the other hand, has an infrared conductivity of $\sigma_{bilayer}$. The optical conductivities of both monolayer and AB-stacked bilayer graphene have been well established in the literature[32]. At the infrared wavelength of 6.1 μm, the value of $2\sigma_{monolayer}$ is about 20% higher than that of $\sigma_{bilayer}$, which can qualitatively explain the bright infrared contrast of the domain walls observed in our studies.

Electrical transport data of four extra bilayer graphene devices. We investigated five bilayer graphene device pairs with a fixed channel length of 1 μm. In Extended Data Fig. 1, we show the complete set of data taken from the four pairs of bilayer graphene devices other than that included in Fig. 3c and d. Each pair of bilayer graphene devices includes one with AB-BA stacking domain walls and one reference device with no domain walls on the same graphene flake. Extended Data Fig. 1a–d displays resistances of corresponding bilayer graphene devices with domain walls, including three single-domain-wall devices (Extended Data Fig. 1a–c) and one double-domain-wall device (Extended Data Fig. 1d). All single-domain-wall devices show resistances saturating at 14 kΩ with increasing D, and the double-domain-wall device has a resistance saturating around 8 kΩ. For comparison, Extended Data Fig. 1e–h displays the gate-dependent resistance for four bilayer graphene devices without boundaries. These devices show continuously increasing CNP resistance to well above 14 kΩ (8 kΩ in Extended Data Fig. 1h), as indicated by the dashed line at high V_{bg}. All the data show that one-dimensional conducting channels are present at AB-BA domain walls, and that they dominate electrical transport in gapped bilayer graphene.

Length dependence of electrical transport along AB-BA domain walls. We investigated two sets of dual-gated bilayer graphene domain wall devices of varying channel lengths (defined by the top gate width). Each set of devices are fabricated on one single domain wall in the same bilayer graphene flake, and includes four channels with lengths of 200 nm, 400 nm, 600 nm and 800 nm, respectively. The complete transport data of these bilayer graphene domain wall devices are shown in Extended Data Fig. 2.

Temperature dependence of electrical transport of AB-BA domain walls. We investigated the temperature dependence of electrical transport both through AB-stacked bilayer graphene and through AB-BA domain walls. Extended Data Fig. 3 displays representative data for CNP resistance at $V_{bg} = -140$ V for a bilayer graphene device without a domain wall (black line) and a device with a domain wall (red line). For the bilayer graphene bulk device without a domain wall, the CNP resistance increases by over 300 kΩ (2.5 times) as the temperature is varied from 50 K to 1.8 K. This large increase of resistance at lower temperatures is characteristic of insulating behaviour. In comparison, the CNP resistance of device with a domain wall (red line) has much weaker temperature dependence: the resistance increase is only 5 kΩ (~50%), and part of the increase is due to the contribution from bulk bilayer graphene channel in parallel with the one-dimensional domain wall channel. The weak temperature dependence of conductance along the domain wall is characteristic of a metallic system.

31. Lopes dos Santos, J. M. B., Peres, N. M. R. & Castro Neto, A. H. Graphene bilayer with a twist: electronic structure. *Phys. Rev. Lett.* **99,** 256802 (2007).
32. Mak, K. F., Sfeir, M. Y., Misewich, J. A. & Heinz, T. F. The evolution of electronic structure in few-layer graphene revealed by optical spectroscopy. *Proc. Natl Acad. Sci. USA* **107,** 14999–15004 (2010).

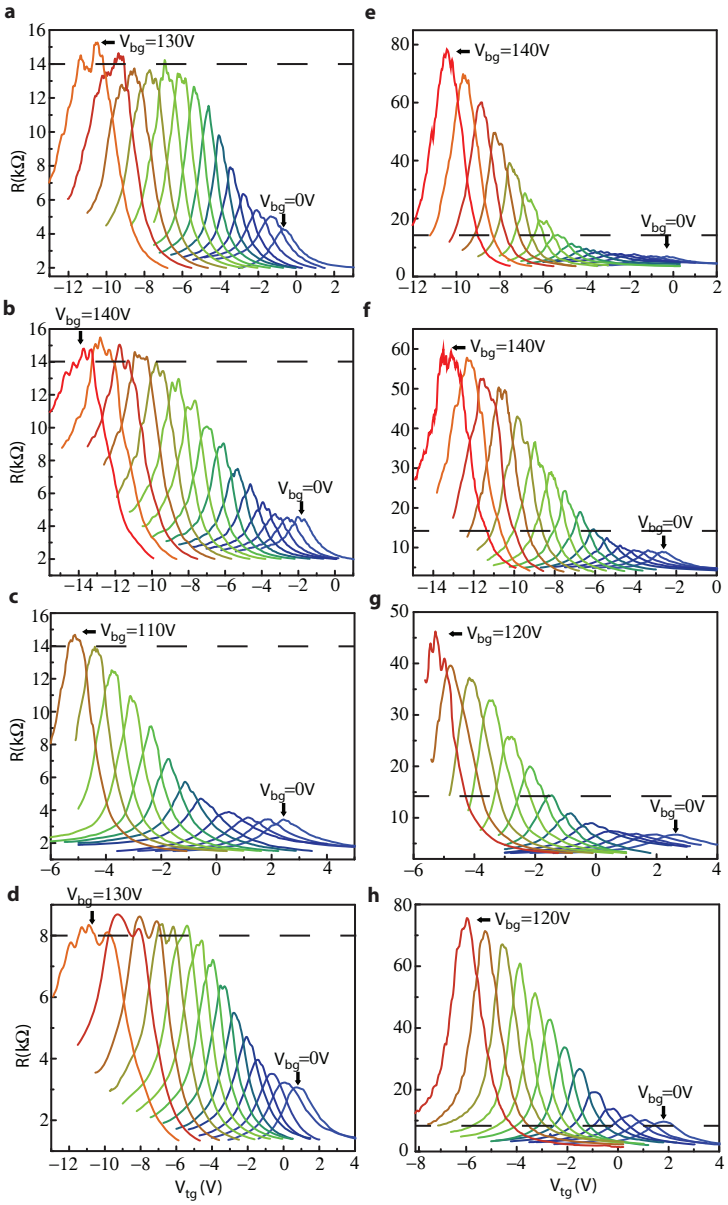

Extended Data Figure 1 | Electrical transport of dual-gated bilayer graphene devices with (left) and without (right) AB-BA domain walls. **a**–**d**, Gate-dependent resistance R for three bilayer graphene devices with one domain wall (**a**–**c**) and one with two domain walls (**d**) at 4.2 K. The backgate voltage V_{bg} is varied from 0 V to 140 V with a step of 10 V, and the top gate voltage V_{tg} is swept continuously. The resistance peak in each trace corresponds to a CNP. The resistance at the CNP first increases and then saturates at ~14 kΩ in **a**–**c** (~8 kΩ in **d**). The dashed lines indicate the saturated conductance values. **e**–**h**, Gate-dependent resistance of four reference bilayer graphene devices without domain walls. The resistance at the CNP increases continuously at high V_{bg} owing to the opening of a bandgap, and reaches values much higher than that of corresponding devices with bilayer graphene domain walls (indicated by the dashed line).

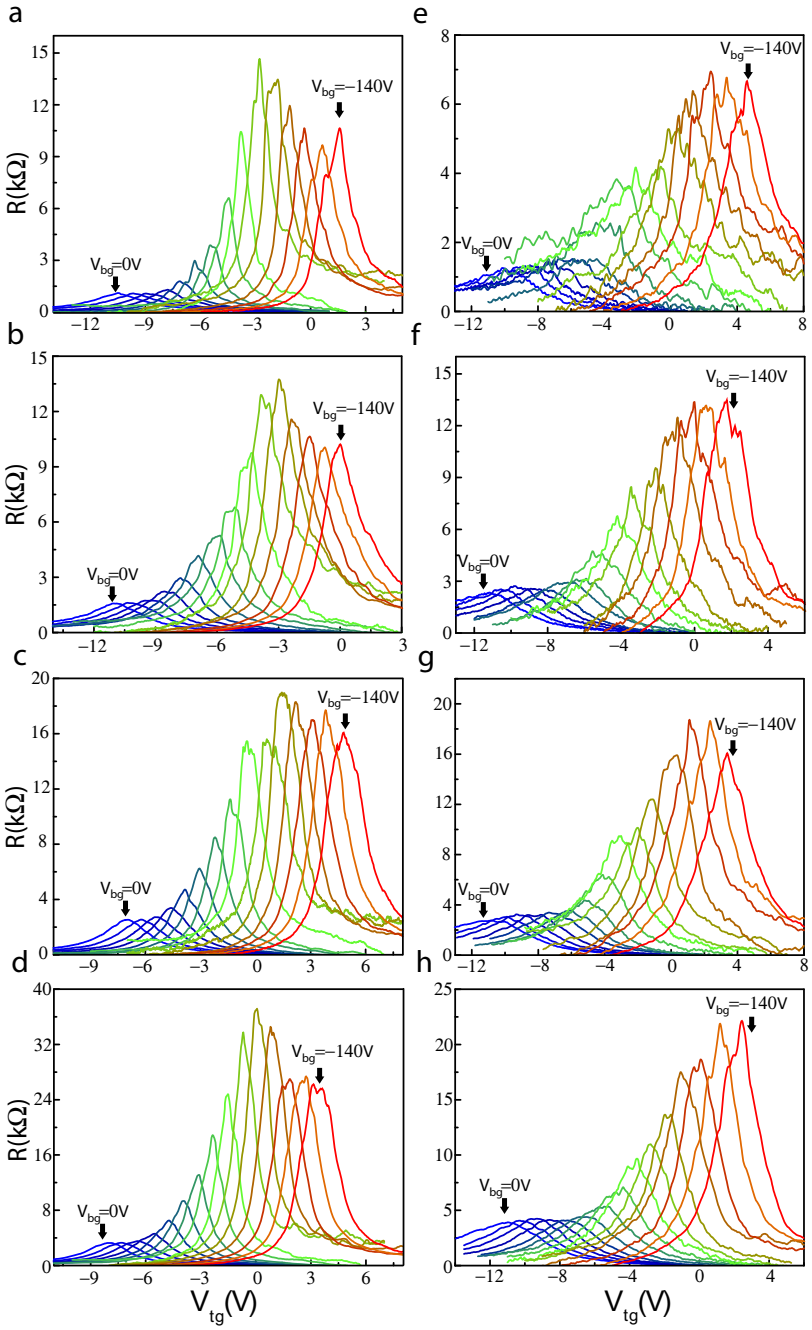

Extended Data Figure 2 | Length dependence of electrical transport of AB-BA domain walls. Data in left panels are from one graphene flake, data in right panels are from another. **a**–**d**, Gate-dependent resistance for four bilayer graphene devices fabricated on a long domain wall with channel lengths of 200 nm, 400 nm, 600 nm and 800 nm (defined by the top gate width), respectively. **e**–**h**, Gate-dependent resistance for four bilayer graphene devices fabricated on another long domain wall with channel lengths of 200 nm, 400 nm, 600 nm and 800 nm respectively. The backgate voltage V_{bg} is varied from 0 to −140 V with a step of 10 V, and the top gate voltage V_{tg} is swept continuously. The resistance peak in each trace corresponds to a CNP. The resistance at the CNP first increases as the bandgap is opened in the bulk and then saturates at high V_{bg}, where the electrical transport is dominated by one-dimensional channels along the domain wall.

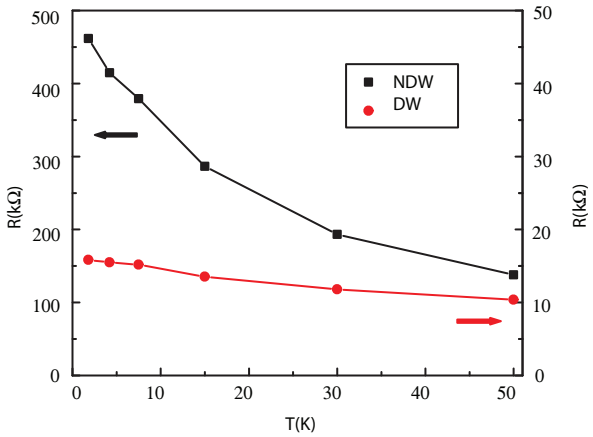

Extended Data Figure 3 | Temperature-dependent electrical transport through bulk bilayer graphene and through the AB-BA domain wall. The CNP resistance ($V_{bg} = -140$ V) of a bilayer graphene device without a domain wall (NDW, black line) increases by over 300 kΩ (~2.5 times) as the temperature is decreased from 50 K to 1.8 K. In contrast, the CNP resistance ($V_{bg} = -140$ V) of a bilayer graphene device with domain wall (red line, the same device as in Extended Data Fig. 2c) increases by only 5 kΩ (~50%) at the same temperature. The much weaker temperature dependence of the domain wall resistance arises from a metallic one-dimensional conducting channel.